AIP | Applied Physics Letters

Enhancement of multiferroic properties of Pb (Fe 1 / 2 Nb 1 / 2) O 3 thin films on SrRuO 3 buffered SrTiO 3 substrates

Li Yan, Xin Zhao, Jiefang Li, and D. Viehland

Citation: Applied Physics Letters **94**, 192903 (2009); doi: 10.1063/1.3138162
View online: http://dx.doi.org/10.1063/1.3138162
View Table of Contents: http://scitation.aip.org/content/aip/journal/apl/94/19?ver=pdfcov
Published by the AIP Publishing

Enhancement of multiferroic properties of $Pb(Fe_{1/2}Nb_{1/2})O_3$ thin films on $SrRuO_3$ buffered $SrTiO_3$ substrates

Li Yan,[a] Xin Zhao, Jiefang Li, and D. Viehland
Department of Materials Science and Engineering, Virginia Tech, Blacksburg, Virginia 24061, USA

(Received 5 February 2009; accepted 25 April 2009; published online 14 May 2009)

We report multiferroic properties of $Pb(Fe_{1/2}Nb_{1/2})O_3$ (or PFN) epitaxial thin layers grown on (001), (110), and (111) $SrTiO_3$ substrates with and without a $SrRuO_3$ (SRO) buffer. Our findings are as follows: (i) the constraint stress on (001) substrates is more than ten times larger than those on (110) and (111); (ii) this large constraint stress induces higher piezoelectric constants, magnetic permeability and magnetization for (001) PFN compared with (110) and (111) layers; (iii) epitaxy distorts the structure of (001) PFN causing the films to be weakly ferromagnetic, whereas (110) films are antiferromagnetic; and (iv) a significant increase of the coercivity of (001) layers occurs due to clamping by a SRO buffer layer. © *2009 American Institute of Physics*.
[DOI: 10.1063/1.3138162]

Lead iron niobate, $Pb(Fe_{1/2}Nb_{1/2})O_3$ (PFN), which was discovered by Smolenskii *et al.* in the 1950s,[1] is rhombohedral with lattice parameters of a_r=4.0123 Å (or 4.058 Å) and α_r=89.89°.[1–4] It is a kind of multiferroic oxide, which draw much attention in the past several years because of the properties and potential applications.[5] It changes from paraelectric to relaxor ferroelectric at a Curie temperature of 385 K.[1,6] PFN crystals undergo a transformation from paramagnetic to antiferromagnetic (AFM) at a Néel temperature of T_{N1}=143 K (Ref. 2) and subsequently undergo a secondary AFM→AFM transition at T_{N2}=19 K.[7,8] It is believed that the PM→AFM transformation is related to a 180° Fe–O–Fe AFM superexchange, whereas the AFM→AFM one is related to a 180 ° Fe–O–Nb–O–Fe superlattice exchange.[8]

Strontium ruthenium oxide, $SrRuO_3$ (SRO), was reported by Randall and Ward in 1958,[9] which is an ideal bottom electrode for other perovskite dielectrics because of its low resistivity.[10,11] SRO has ferromagnetic (FM) order below a Curie temperature of T_c=160 K.[12] The anisotropy of SRO thin films has previously been studied, where the coercivity can vary from 2 to 10 kOe for variously oriented layers grown under different deposition conditions.[13–15]

Multiferroic properties of epitaxial thin films may be changed by constraint stress imposed by the substrate on thin layers. For example, the saturation polarization of $BiFeO_3$ and $BaTiO_3$ thin films can be increased to approximately 100 and 80 $\mu C/cm^2$, respectively, by substrate constraint.[16,17] It was found that $Pb(Zr_{0.53}Ti_{0.47})O_3$ thin film can vary from *a*-domain dominated to *c*-domain dominated structures by changing the tensile stress to a compressive stress, which were imposed by the substrate at the Curie temperature. By doing so, the ferroelectric properties increased notably, which may result in a significant improvement in the piezoresponse.[18] FM properties of ferrite thin films can be changed by said constraint stress.[19,20] In addition, the magnetization can be altered by magnetic coupling to a FM or AFM buffer layer. Here, we show how the multiferroic properties of PFN epitaxial layers are altered by constraint stress, and in addition, by an exchange with a SRO buffer layer.

Epitaxial thin layers of PFN were deposited on $SrTiO_3$ (STO) substrates with (and without) a SRO buffer layer by pulsed laser deposition. The energy density of the KrF laser (Lambda 305i) was 1.2 J/cm^2, and the distance between target and substrate was 6 cm. A bottom SRO thin film was deposited on the STO substrate at 660 °C. Films of PFN were then deposited at 630 °C. The base vacuum of the chamber was $<10^{-5}$ Torr. During film deposition, the oxygen pressure was 150 mTorr for SRO and 20 mTorr for PFN. The crystal structure of the films was measured using a Philips X'pert diffractometer equipped with a two-bounce hybrid monochromator and an open three-circle Eulerian cradle. The piezoelectricity of the PFN layers was measured by a piezoforce microscope (Veeco Dimension 3100). The magnetization of the thin films was determined by a Quantum Design superconducting quantum interface device (SQUID). We deposited and characterized three sets of samples which were grown on (001), (110), and (111) STO. These are designated as S1, S2, and S3. S1 were 200 nm PFN films deposited on STO substrates, S2 were 200 nm PFN films deposited on top of a 50 nm SRO buffer layer grown on STO substrates, and S3 were 400 nm PFN films deposited on top of a 50 nm SRO buffer grown on STO substrates. The thicknesses of the thin films were controlled by the deposition time and were measured by scanning electron microscopy.

We need to determine the in-plane constraint stress of PFN thin films for the variously oriented substrates. The generalized Hooke's law is as follows:

$$\varepsilon_x = \frac{1}{E}[\sigma_x - \upsilon(\sigma_y + \sigma_z)], \quad \varepsilon_y = \frac{1}{E}[\sigma_y - \upsilon(\sigma_x + \sigma_z)], \quad \varepsilon_z = \frac{1}{E}[\sigma_z - \upsilon(\sigma_x + \sigma_y)], \tag{1}$$

where ε_i is the strain tensor, σ_i is the stress tensor, E is Young's modulus, and υ is Poisson's ratio. In the thin film, σ_z=0, $\varepsilon_i = a_i - a_0/a_0$, where a_i is the equivalent lattice constant of thin film in i (x, y, or z) directions. In our calculation, PFN was assumed to be pseudocubic at room temperature, with a lattice constant of $a_0 = \sqrt[3]{V}$. Accordingly, the in-plane stress imposed on the PFN thin film by the substrate simplifies to

[a]Electronic mail: lyan@vt.edu.

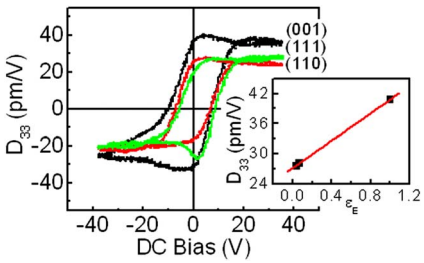

FIG. 1. (Color online) Piezoresponse hysteresis loops for (001), (110), and (111) oriented PFN thin films. Inset shows the piezocoefficients as a function of in-plane strain. The data illustrate that the d_{33} of (001) PFN thin film is much higher than the other two orientations.

$$\sigma_{\text{in-plane}} = \frac{\sigma_x+\sigma_y}{2} = E\left(\frac{a_x+a_y-a_z-a_0}{2a_0}\right) = E\varepsilon_E, \tag{2}$$

where $\varepsilon_E=(a_x+a_y-a_z-a_0/2a_0)$ is proportional to $\sigma_{\text{in-plane}}$ and is defined as the equivalent in-plane strain. This estimate of $\sigma_{\text{in-plane}}$ is more accurate for calculations than the widely used lattice mismatch, $(a_{\text{film}}-a_{\text{substrate}}/a_{\text{substrate}})$, which accounts for in-plane stress between substrate and epitaxial layer. The value of ε_E was -1.0×10^{-2}, -6.3×10^{-4}, and -3.8×10^{-4} for 200 nm (001), (110), and (111) oriented PFN thin films, respectively. Detailed measurements and calculations of the lattice constants of PFN thin films are given in Ref. 21. The negative values mean that the constraint stress is compressive. Please note that the in-plane constraint stress on (001) is more than ten times larger than that on (110) and (111).

The piezoresponse hysteresis loops for differently oriented PFN thin films (S2) are shown in Fig. 1. In these measurements, the ac voltage was 2 V at 6 kHz (which was the resonant frequency of the PFN thin film). The coercive field can be seen to be 7 V. The value of the piezoelectric coefficient d_{33} for (001) oriented PFN thin film was much higher than the other orientations, reaching a maximum value of 40 pm/V for $V>15$ V; whereas, d_{33} for (110) and (111) PFN thin films was 28 pm/V. Comparisons of these findings to our estimates for $\sigma_{\text{in-plane}}$ reveal that larger constraint stress as result in more strongly piezoelectric layers.

Next, the temperature dependence of the magnetization of S1 is shown for variously oriented 200 nm PFN films, as given in Fig. 2. The films were zero-field cooled to 5 K, and the magnetization measured on heating under a magnetic field of 2×10^3 Oe. The temperature dependence of the slope of the magnetization (i.e., the magnetic susceptibility) is then shown as an inset in this figure. These data reveal a

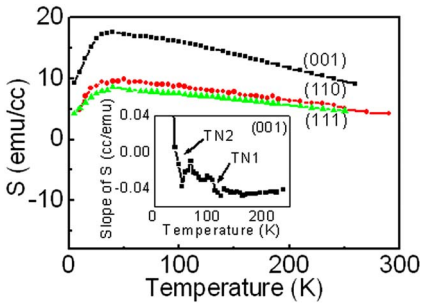

FIG. 2. (Color online) Permeability of (001), (110), and (111) oriented PFN films. The data illustrate that the permeability of (001) PFN is much higher than the other orientations. The inset shows the temperature dependence of the magnetic permeability determined from the slope.

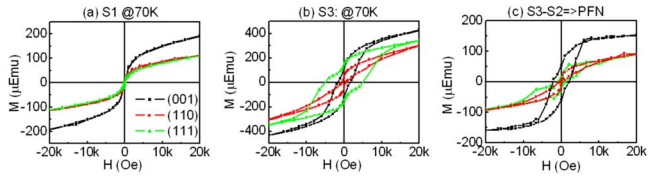

FIG. 3. (Color online) The *M-H* loops taken using a SQUID for (a) S1 (200 nm PFN), (b) S3 (400 nm PFN/50 nm SRO), and (c) S3-S2. The data show the magnetic properties of (001), (110), and (111) oriented PFN, PFN/SRO, and PFN (on top of SRO) thin films, respectively.

sequence of two magnetic phase transitions with Néel temperatures of $T_{N1}\approx50$ K and $T_{N2}\approx125$ K, and are consistent with prior investigations of PFN single crystals.[3] The results given in Fig. 2 indicate that the phase transformational sequences of PFN thin layers are not altered by epitaxial mismatch. However, the magnitude of the susceptibility for (001), (110), and (111) PFN thin films were 16, 9, and 8 emu/cc at 70 K, respectively. We can see that the susceptibility of (001) PFN is much larger than that of (110) and (111), which was induced by higher constraint stress on (001) STO substrates.

Finally, we measured the in-plane *M-H* response for the various films. Figure 3(a) shows data for S1: PFN (200 nm)/STO at 70 K. The induced magnetization was 190 μemu for (001) PFN at a field of $H=2$ kOe, and 110 μemu for (110) and (111) PFN. These data show that the induced magnetization is notably dependent on $\sigma_{\text{in-plane}}$: the higher the stress, the larger the magnetization. This finding is consistent with the stabilization of an AFM spin order with a weak ferromagnetism induced by distortion of the crystal. The $\sigma_{\text{in-plane}}$ imposed by the substrate tilts the Fe–O–Fe or Fe–O–Nb–O–Fe bond angle away from 180° (which favors AFM order). The larger this tilt, the more pronounced the weak ferromagnetism becomes, which is proportional to $\cos^2\theta$.[22–25]

Figure 3(b) shows the *M-H* curves for S3, PFN (400 nm)/SRO (50 nm), grown on various oriented STO substrates. These measurements were performed at 70 K and measured with the field applied parallel to the plane of the films. The SRO thin films are magnetically hard compared with the PFN ones, i.e., they have relatively square *M-H* loops and high values of H_C. Accordingly, on reversal of the spin direction under field, the spin of PFN reverses at lower magnetic fields: only when $H>H_C$ does the spin direction of the SRO layer reverse. It was observed that there are two steps in the *M-H* curves for S3, corresponding to spin rotation in both SRO and PFN magnetic layers. By subtracting the value of the magnetization of S2 from that of S3, we attempted to estimate the value of the magnetization of the 200 nm PFN layer in S3. The results are shown in Fig. 3(c). For the variously oriented films, the saturation magnetization was estimated to be 160 and 100 μemu for (001) and (110)/(111) oriented PFN thin films, respectively, which is similar to that for S1 [PFN (200 nm)/STO]. From these data, it can be clearly seen that the (001) layer in all cases has a larger magnetic moment with a weak FM order. The (110) and (111) layers have a much smaller in-plane constraint stress, and correspondingly the structural distortions induced in the layers are much smaller than for (001) ones. In this case apparently, a homogeneous AFM spin order is preferred over that with a weak FM one. Furthermore, the value of the coercive field for S2 was $H_C=2$ kOe, which was much

larger than that for S1. This notable increase in H_C can be attributed to a spin clamping of the PFN layer by exchange coupling with the SRO buffer layer.

In summary, the effect of in-plane constraint stress has been studied for PFN epitaxial thin films grown on various oriented STO substrates. It was found that $\sigma_{\text{in-plane}}$ enhances the piezoelectric constant, magnetic permeability, and magnetization. These enhancements were strongest for (001) layers, i.e., $(001) > (110) \approx (111)$. In general, the larger $\sigma_{\text{in-plane}}$, the higher the multiferroic properties. We attribute these enhancements in piezoelectricity and weak ferromagnetism to distortions of the crystal structures of PFN induced by epitaxial constraint.

We gratefully acknowledge financial support from the U.S. Department of Energy under Contract No. DE-AC02-98CH10886 and the Office of the Air-Force Office of Scientific Research under Contract No. FA 9550-06-1-0410.

[1]G. A. Smolenskii, A. Agranovskaya, S. N. Popov, and V. A. Isupov, Sov. Phys. Tech. Phys. **28**, 2152 (1958).
[2]V. A. Bokov, I. E. Mylnikova, and G. A. Smolenskii, Sov. Phys. JETP **15**, 447 (1962).
[3]Y. Yang, J. M. Liu, H. B. Huang, W. Q. Zou, P. Bao, and Z. G. Liu, Phys. Rev. B **70**, 132101 (2004).
[4]Y. Yang, S. T. Zhang, H. B. Huang, Y. F. Chen, Z. G. Liu, and J. M. Liu, Mater. Lett. **59**, 1767 (2005).
[5]W. Prellier, M. P. Singh, and P. Murugavel, J. Phys.: Condens. Matter **17**, R803 (2005).
[6]G. L. Platonov, L. A. Drobyshev, Y. Y. Tomashpolskii, and Y. N. Venevtsev, Sov. Phys. Crystallogr. **14**, 692 (1970).
[7]T. Watanabe and K. Kohn, Phase Transit. **15**, 57 (1989).
[8]V. V. Bhat, K. V. Ramanujachary, S. E. Lofland, and A. M. Umarji, J. Magn. Magn. Mater. **280**, 221 (2004).
[9]J. J. Randall and R. Ward, J. Am. Chem. Soc. **81**, 2629 (1959).
[10]R. J. Bouchard, and J. L. Gillson, Mater. Res. Bull. **7**, 873 (1972).
[11]C. B. Eom, R. J. Cava, R. M. Fleming, J. M. Phillips, R. B. van Dover, J. H. Marshall, J. W. P. Hsu, J. J. Krajewski, and W. F. Peck, Jr., Science **258**, 1766 (1992).
[12]A. Callaghan, C. W. Moeller, and R. Ward, Inorg. Chem. **5**, 1572 (1966).
[13]Q. Gan, R. A. Rao, C. B. Eom, L. Wu, and F. Tsui, J. Appl. Phys. **85**, 5297 (1999).
[14]R. A. Rao, D. B. Kacedon, and C. B. Eom, J. Appl. Phys. **83**, 6995 (1998).
[15]S. Kolesnik, Y. Z. Yoo, O. Chmaissem, B. Dabrowski, T. Maxwell, C. W. Kimball, and A.P. Genis, J. Appl. Phys. **99**, 08F501 (2006).
[16]J. Wang, J. B. Neaton, H. Zheng, V. Nagarajan, S. B. Ogale, B. Liu, D. Viehland, V. Vaithyanathan, D. G. Schlom, U. V. Waghmare, N. A. Spaldin, K. M. Rabe, M. Wuttig, and R. Ramesh, Science **299**, 1719 (2003).
[17]K. J. Choi, M. Biegalski, Y. L. Li, A. Sharan, J. Schubert, R. Uecker, P. Reiche, Y. B. Chen, X. Q. Pan, V. Gopalan, L. Q. Chen, D. G. Schlom, and C. B. Eom, Science **306**, 1005 (2004).
[18]B. Tuttle, T. Headley, C. Drewien, J. Michael, J. Voigt, and T. Garino, Ferroelectrics **221**, 209 (1999).
[19]Q. Gan, R. A. Rao, C. B. Eom, J. L. Garrett, and M. Lee, Appl. Phys. Lett. **72**, 978 (1998).
[20]N. Wakiya, K. Shinozaki, and N. Mizutani, Appl. Phys. Lett. **85**, 1199 (2004).
[21]L. Yan, J. F. Li, and D. Viehland, J. Mater. Res. **23**, 663 (2008).
[22]K. Motida and S. Miyahara, J. Phys. Soc. Jpn. **28**, 1188 (1970).
[23]G. A. Sawatzky, W. Geertsma, and C. Haas, J. Magn. Magn. Mater. **3**, 37 (1976).
[24]J. Kanamori, J. Phys. Chem. Solids **10**, 87 (1959).
[25]J. B. Goodenough, Phys. Rev. **100**, 564 (1955).